Epitaxial Al_2O_3 capacitors for low microwave loss superconducting quantum circuits

K.-H. Cho, U. Patel, J. Podkaminer, Y. Gao, C. M. Folkman, C. W. Bark, S. Lee, Y. Zhang, X. Q. Pan, R. McDermott, and C. B. Eom

Citation: APL Materials **1**, 042115 (2013); doi: 10.1063/1.4822436

View online: https://doi.org/10.1063/1.4822436

View Table of Contents: http://aip.scitation.org/toc/apm/1/4

Published by the American Institute of Physics

APL MATERIALS **1**, 042115 (2013)

Epitaxial Al_2O_3 capacitors for low microwave loss superconducting quantum circuits

K.-H. Cho,[1] U. Patel,[2] J. Podkaminer,[1] Y. Gao,[2] C. M. Folkman,[1] C. W. Bark,[1] S. Lee,[1] Y. Zhang,[3] X. Q. Pan,[3] R. McDermott,[2] and C. B. Eom[1,a]

[1]*Department of Materials Science and Engineering, University of Wisconsin, Madison, Wisconsin 53706, USA*
[2]*Department of Physics, University of Wisconsin, Madison, Wisconsin 53706, USA*
[3]*Department of Materials Science and Engineering, University of Michigan, Ann Arbor, Michigan 48109, USA*

(Received 12 June 2013; accepted 22 August 2013; published online 21 October 2013)

We have characterized the microwave loss of high-Q parallel plate capacitors fabricated from thin-film $Al/Al_2O_3/Re$ heterostructures on (0001) Al_2O_3 substrates. The superconductor-insulator-superconductor trilayers were grown *in situ* in a hybrid deposition system: the epitaxial Re base and polycrystalline Al counterelectrode layers were grown by sputtering, while the epitaxial Al_2O_3 layer was grown by pulsed laser deposition. Structural analysis indicates a highly crystalline epitaxial Al_2O_3 layer and sharp interfaces. The measured intrinsic (low-power, low-temperature) quality factor of the resonators is as high as 3×10^4. These results indicate that low-loss grown Al_2O_3 is an attractive candidate dielectric for high-fidelity superconducting qubit circuits. [http://dx.doi.org/10.1063/1.4822436]

Superconducting phase qubits are a promising candidate for scalable quantum computing in the solid state.[1–6] The phase qubit has achieved several notable milestones, including realization of high-fidelity entangling gates in two and three qubit circuits,[3] quantum state tomography of two and three qubits,[3,4] and full characterization of highly non-classical states in linear microwave resonators.[5,6] However, qubit gate fidelity is limited by relatively short energy relaxation times of order hundreds of ns.[7] It has been shown that the energy relaxation rate is dominated by spurious coupling of the qubit to low-energy two-level state (TLS) defects in the amorphous dielectrics of the qubit circuit.[8] These defects are believed to arise from atomic scale structural imperfections[9] and are known to exist in the surface oxides of the superconductors, at the superconductor-insulator interface, and in the bulk of the amorphous dielectrics of the circuit.[10,11] There are ongoing efforts to develop improved low-loss amorphous dielectric materials for superconducting qubits,[12,13] and it is expected that the incorporation of defect-free, crystalline dielectrics into qubit circuits will lead to dramatic improvements in energy relaxation times. There have been prior efforts to realize Josephson tunnel barriers from grown epitaxial Al_2O_3 and phase qubits incorporating crystalline junctions display a factor 5 reduction in the density of resonant TLS junction defects.[14] Furthermore, there have been efforts to incorporate epitaxial Josephson junctions into the transmon qubit.[15,16] However, this approach to qubit realization requires excellent control over the grown tunnel barrier thickness, which determines the junction critical current. An alternative approach is to fabricate a submicrometer Josephson junction and to shunt the junction with a low-loss external capacitance.[17] In this approach, qubit T_1 is very simply related to the loss tangent of the capacitor dielectric: $T_1 = 1/\omega_{10} \tan\delta$, where ω_{10} is the qubit transition frequency.

[a]Electronic mail: eom@engr.wisc.edu

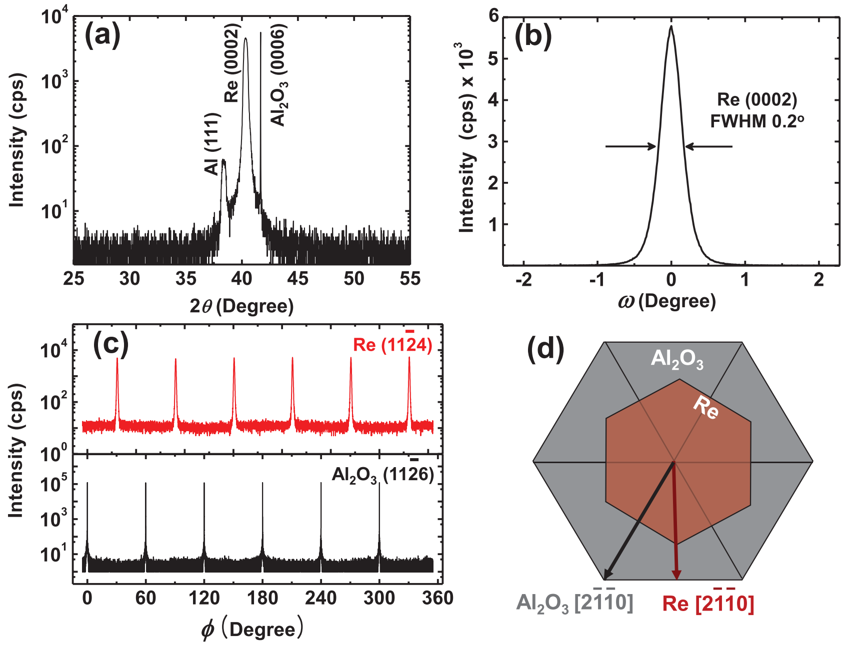

FIG. 1. (a) X-ray diffraction θ-2θ scan of the Al/Al_2O_3/Re trilayer on (0001) Al_2O_3 substrate. (b) Rocking curve θ-scan of the (0002) Re reflection. (c) X-ray azimuthal ϕ-scans of the Al_2O_3 $(11\bar{2}6)$ and Re $(11\bar{2}4)$ reflections. (d) Schematic diagram of $[2\bar{1}\bar{1}0]$ Al_2O_3//$[10\bar{1}0]$ Re in-plane relationship between Al_2O_3 substrate and Re film.

Here, we report the development of crystalline Al/Al_2O_3/Re trilayers for potential applications as qubit shunt capacitors. As has been shown previously, rhenium (Re) is an attractive candidate for epitaxial qubit applications since it has a low free energy of oxidation, a high melting temperature, and an excellent lattice match to sapphire, factors that are crucial to the realization of a high-quality metal-dielectric interface.[14,18] Moreover, optimized Re films have very low microwave loss.[19]

The epitaxial trilayers were grown in a custom hybrid deposition system incorporating both pulsed laser deposition (PLD) and planar magnetron sputtering sources, switchable by a simple $\sim$180° rotation of the substrate heater.[20] The hybrid system was further equipped with high-pressure reflection high-energy electron diffraction (RHEED),[21] which enabled *in situ* surface monitoring during the growth. The trilayers were grown on single crystal c-plane Al_2O_3 substrates (Crystec GmbH Berlin, Germany). Prior to Re deposition, the Al_2O_3 substrates were annealed in a flowing O_2 environment at 1100 °C for 4 h. The 100 nm-thick epitaxial Re base layers were deposited at 900 °C via dc magnetron sputtering from a 1.33″ diameter Re target (purity > 99.99%); following growth, the films were annealed in vacuum at 900 °C for 2 h. Next, the Al_2O_3 dielectric layers were grown by PLD from a 1″ diameter, 1/8″ thick ceramic target; the PLD system employed a KrF excimer laser ($\lambda = 248$ nm) operating at 5 Hz with a fluence of 1.2 J/cm^2. We investigated two different processes for Al_2O_3 growth. In the first approach (the "one-step" process), a 20 nm-thick Al_2O_3 film was deposited at 850 °C in a single step. In the second approach (the "two-step" process), we first grew 2 nm of amorphous AlO_x at room temperature; we then annealed the sample in vacuum at 850 °C to form a seed layer for Al_2O_3 homoepitaxy and deposited an additional 18 nm of Al_2O_3 at that temperature. To complete the trilayer, a 100 nm-thick Al layer was grown by dc magnetron sputtering at room temperature.

The crystalline quality and epitaxial arrangement of the thin films was investigated by conventional four-circle XRD using Cu$K_{\alpha 1}$ radiation (Bruker D8). The one-step grown Al_2O_3 layers on Re are aligned epitaxially and show no sign of a second phase. In Fig. 1(a), the 2θ-θ scan shows that both the Re and the one-step deposited Al_2O_3 layers grow with the c-axis normal to the substrate. From the measurements, Re lattice parameters $a_0 = 2.77$ Å and $c_0 = 4.47$ Å were determined,

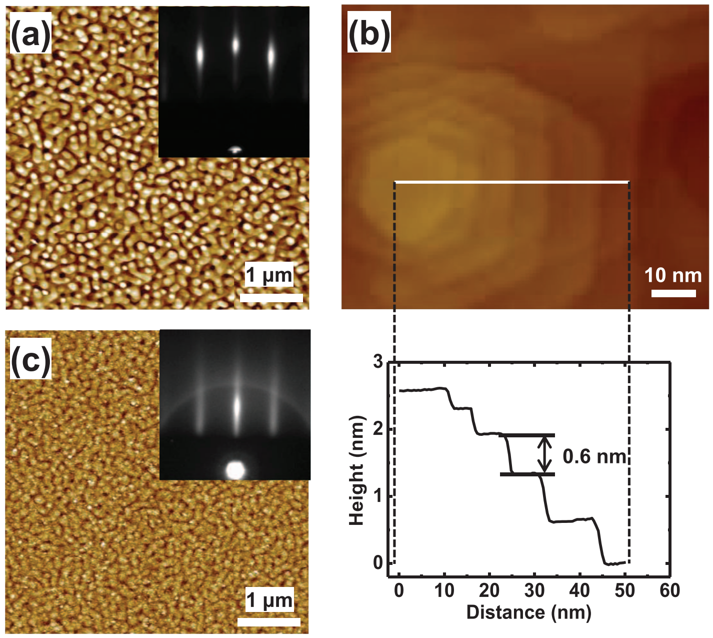

FIG. 2. AFM image and RHEED pattern of the grown Re and Al_2O_3 layers: (a) Epitaxial Re on Al_2O_3 substrate and (b) STM image of 100 nm-thick Re film showing single unit cell steps. The line scan of STM image of Re film. (c) AFM image and RHEED pattern of epitaxial Al_2O_3 layer on Re/Al_2O_3 substrate.

indicating full relaxation with the same unit cell volume as bulk Re.[22] The full width at half maximum (FWHM) value in (0002) Re rocking curve is 0.2°, which is narrower than any previously reported value to the best of our knowledge [Fig. 1(b)]. Fig. 1(c) shows azimuthal ϕ-scans of the off-axis $(11\bar{2}6)$ Al_2O_3 substrate and $(11\bar{2}4)$ Re reflections, which exhibit a 30° in-plane rotation of the Re with respect to Al_2O_3.[23] The schematic diagram of the in-plane relationship between Re and Al_2O_3 layer is shown in Fig. 1(d). We grew a 20 nm-thick Al_2O_3 layer on top of the Re/Al_2O_3 substrate while maintaining the same in- and out-of-plane epitaxial alignment with the Al_2O_3 substrate and without any sign of peak separation in 2θ-θ and ϕ-scans (not shown).

Figs. 2(a) and 2(c) show AFM images and RHEED patterns of the epitaxial Re and one-step grown Al_2O_3 films, respectively. The films display island growth with characteristic lateral dimensions from 100 to 150 nm. The rms roughness of the Re and Al_2O_3 thin films are 0.7 nm and 1.6 nm, respectively. The RHEED patterns of the Re and the Al_2O_3 thin film show bright streaks, indicating that the heteroepitaxy proceeds in a Frank-Van der Merwe (FV) growth mode, yielding a high degree of crystallinity. We see hexagonal islands comprising single unit cell steps centered on screw dislocations. The hexagonal islands in the Re films have screw dislocations at the center as revealed by the STM image shown in Fig. 2(b). This indicates that the growth proceeds in a spiral mode with the screw dislocation as the growth flow axis. As shown in Fig. 2(b), observed step is 0.3 nm high. The line scan covers two single steps and three double steps, showing a height of ∼2.4 nm.

We have used TEM analysis to confirm the epitaxial growth of the trilayer heterostructure. Fig. 3(a) shows a low magnification bright-field TEM image. In Fig. 3(b), the high-resolution TEM image shows an atomically sharp interface between the Re and Al_2O_3 layers; the epitaxial match between the layers is clear. Fig. 3(c) shows the selected area electron diffraction pattern (SAED) of the Al_2O_3 thin film on Re from a planar view. The diffraction pattern shows only one set of Al_2O_3 spots, which overlap with the Re spots. The elongation of the diffraction spots indicates small angular mosaic spread (<7°) between Al_2O_3 grains. The in-plane epitaxial relationship between the various layers appears to be Al_2O_3 thin film $[\bar{2}110]$//Re $[\bar{1}010]$//Al_2O_3 substrate $[\bar{2}110]$; these relative orientations are also supported by the XRD data.

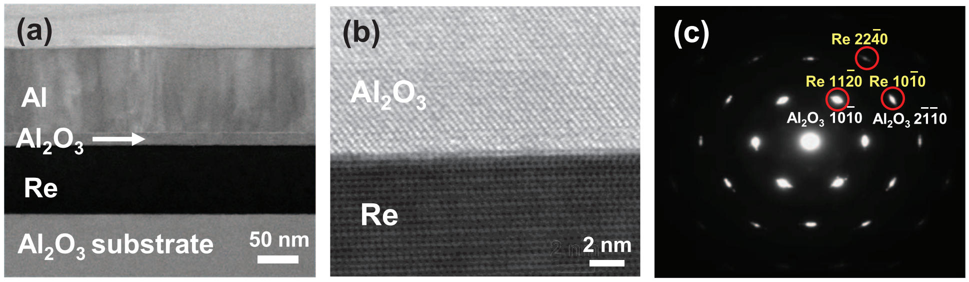

FIG. 3. (a) Low magnification cross-sectional TEM images of Al/Al_2O_3/Re trilayer on (0001) Al_2O_3 substrate. (b) The cross-sectional HRTEM image near the interface between Al_2O_3 thin film and Re layer. (c) Planar view selected area electron diffraction (SAED) pattern of Al_2O_3 thin film and Re layer.

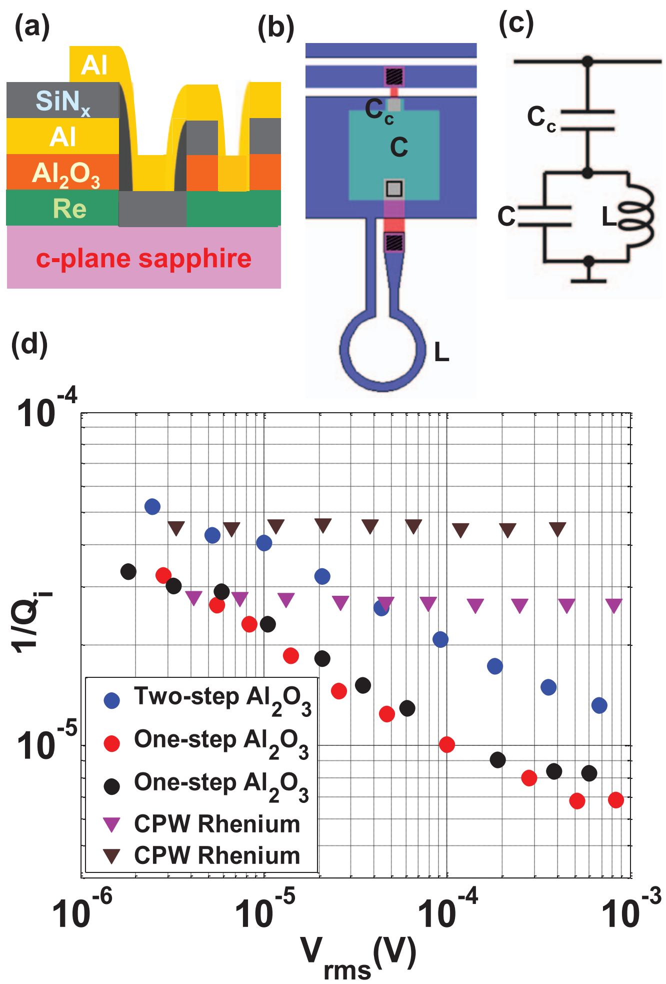

FIG. 4. (a) Layer stack of the lumped element LC resonator device showing epitaxial trilayer and SiN_x overlap coupling capacitor connected to the measurement feedline. The thicknesses for trilayer stack were 100 nm, 20 nm, and 100 nm for Re, Al_2O_3, and Al, respectively. (b) Resonator CAD layout. (c) Electrical circuit schematic of the resonator. (d) Internal loss $1/Q_i$ of epitaxial Re/Al_2O_3/Al *LC* resonators and CPW Re resonators *versus* rms voltage across the resonator. The *LC* resonators incorporate trilayers grown according to both the one-step and two-step processes described in the text; the multiple datasets for the one-step growth and for the CPW Re represent different growth and fabrication runs with nominally identical parameters.

In order to evaluate the dependence of dielectric quality on the growth parameters of the Al_2O_3 films, we fabricated lumped element *LC* resonators from the Al/Al_2O_3/Re stack. Here, the single-turn inductor was fabricated from the Re base layer, and the parallel-plate capacitor incorporated the grown Al_2O_3 layer as the dielectric. The *LC* tank circuits were coupled to a common feedline *via* overlap coupling capacitors comprising an *ex situ* PECVD deposited amorphous SiN_x dielectric as shown in Fig. 4(a). The resonance frequencies of the fabricated resonators were in the range from 4 to 5 GHz. The samples were cooled down in an adiabatic demagnetization refrigerator (ADR) with a base temperature around 50 mK. From the measured frequency-dependent transmission across the resonator we extracted both the loaded and internal quality factors Q_c and Q_i, respectively.[12]

Figure 4(d) shows the internal quality factors of several devices grown under a variety of conditions. The low-power internal quality factor of the resonator incorporating the two-step grown Al_2O_3 is 2×10^4, while the internal Q of the resonator comprising the one-step grown Al_2O_3 is 3×10^4. The measured quality of the one-step grown Al_2O_3 is thus comparable to the intrinsic Q of the best demonstrated amorphous a-Si:H dielectrics.[12] According to the theory of dielectric loss induced by low-energy TLS defects, the dielectric quality factor is expected to scale linearly with the rms voltage across the resonator at high drive power.[24] The extremely weak power dependence observed here suggests that resonator loss is not dominated by low-energy defects in the grown Al_2O_3 films; indeed, separate measurements reveal comparable internal quality factors in single-layer coplanar waveguide resonators (CPW) fabricated from the grown Re layer. It is possible that the low-angle grain boundaries contribute significantly to the loss in both resonator structures; and that the intrinsic quality of the grown Al_2O_3 is significantly higher than the measured internal Q of the *LC* resonators. We anticipate that it will be possible to suppress the loss of the Re thin films in future work.

In summary, we have grown high quality epitaxial Al_2O_3/Re heterostructures on (0001) Al_2O_3 substrates in a hybrid thin film deposition system incorporating both pulsed laser deposition and sputtering. We have investigated the low-temperature, low-power microwave loss properties of the grown trilayers and demonstrated internal quality factors comparable to the best intrinsic Q yet demonstrated for grown dielectric thin films. Our grown epitaxial Al_2O_3 shows promise as a high-quality capacitor dielectric for Josephson phase qubit circuits. The incorporation of low-loss, defect-free crystalline dielectrics into the phase qubit will yield a substantial improvement in qubit energy relaxation time.

We acknowledge funding from the National Science Foundation through Grant No. DMR-0805051, IARPA through Grant No. W911NF-09-1-0368, and DOE Office of Basic Energy Sciences under Award No. DE-FG02-06ER46327 (Superconducting thin film growth). This work was performed in part at the Cornell NanoScale Facility, a member of the National Nanotechnology Infrastructure Network, which is supported by the National Science Foundation (Grant No. ECS-0335765).

[1] M. Devoret and J. M. Martinis, Quantum Inf. Process. **3**, 163–203 (2004).
[2] M. Ansmann, H. Wang, R. C. Bialczak, M. Hofheinz, E. Lucero, M. Neeley, A. D. O'Connell, D. Sank, M. Weides, J. Wenner, A. N. Cleland, and J. M. Martinis, Nature (London) **461**, 504–506 (2009).
[3] M. Neeley, R. C. Bialczak, M. Lenander, E. Lucero, M. Mariantoni, A. D. O'Connell, D. Sank, H. Wang, M. Weides, J. Wenner, Y. Yin, T. Yamamoto, A. N. Cleland, and J. M. Martinis, Nature (London) **467**, 570–573 (2010).
[4] M. Steffen, M. Ansmann, R. C. Bialczak, N. Katz, E. Lucero, R. McDermott, M. Neeley, E. M. Weig, A. N. Cleland, and J. M. Martinis, Science **313**, 1423–1425 (2006).
[5] M. Hofheinz, E. M. Weig, M. Ansmann, R. C. Bialczak, E. Lucero, M. Neeley, A. D. O'Connell, H. Wang, J. M. Martinis, and A. N. Cleland, Nature (London) **454**, 310–314 (2008).
[6] M. Hofheinz, H. Wang, M. Ansmann, R. C. Bialczak, E. Lucero, M. Neeley, A. D. O'Connell, D. Sank, J. Wenner, J. M. Martinis, and A. N. Cleland, Nature (London) **459**, 546 (2009).
[7] E. Lucero, M. Hofheinz, M. Ansmann, R. C. Bialczak, N. Katz, M. Neeley, A. D. O'Connell, H. Wang, A. N. Cleland, and J. M. Martinis, Phys. Rev. Lett. **100**, 247001 (2008).
[8] J. M. Martinis, K. B. Cooper, R. McDermott, M. Steffen, M. Ansmann, K. Osborn, K. Cicak, S. Oh, D. P. Pappas, R. W. Simmonds, and C. C. Yu, Phys. Rev. Lett. **95**, 210503 (2005).
[9] W. A. Phillips, Rep. Prog. Phys. **50**, 1657 (1987).
[10] J. Gao, M. Daal, A. Vayonakis, S. Kumar, J. Zmuidzinas, B. Sadoulet, B. A. Mazin, P. K. Day, and H. G. LeDuc, Appl. Phys. Lett. **92**, 152505 (2008).
[11] J. Gao, J. Zmuidzinas, B. A. Mazin, H. G. LeDuc, and P. K. Day, Appl. Phys. Lett. **90**, 102507 (2007).

[12] A. D. O'Connell, M. Ansmann, R. C. Bialczak, M. Hofheinz, N. Katz, E. Lucero, C. McKenney, M. Neeley, H. Wang, E. M. Weig, A. N. Cleland, and J. M. Martinis, Appl. Phys. Lett. **92**, 112903 (2008).
[13] H. Paik and K. D. Osborn, Appl. Phys. Lett. **96**, 072505 (2010).
[14] S. Oh, K. Cicak, J. S. Kline, M. A. Sillanpää, K. D. Osborn, J. D. Whittaker, R. W. Simmonds, and D. P. Pappas, Phys. Rev. B **74**, 100502 (2006).
[15] M. P. Weides, J. S. Kline, M. R. Vissers, M. O. Sandberg, D. S. Wisbey, B. R. Johnson, T. A. Ohki, and D. P. Pappas, Appl. Phys. Lett. **99**, 262502 (2011).
[16] Y. Nakamura, H. Terai, K. Inomata, T. Yamamoto, W. Qiu, and Z. Wang, Appl. Phys. Lett. **99**, 212502 (2011).
[17] M. Steffen, M. Ansmann, R. McDermott, N. Katz, R. C. Bialczak, E. Lucero, M. Neeley, E. M. Weig, A. N. Cleland, and J. M. Martinis, Phys. Rev. Lett. **97**, 050502 (2006).
[18] S. Oh, D. A. Hite, K. Cicak, K. D. Osborn, R. W. Simmonds, R. McDermott, K. B. Cooper, M. Steffen, J. M. Martinis, and D. P. Pappas, Thin Solid Films **496**, 389–394 (2006).
[19] H. Wang, M. Hofheinz, J. Wenner, M. Ansmann, R. C. Bialczak, M. Lenander, E. Lucero, M. Neeley, A. D. O'Connell, D. Sank, M. Weides, A. N. Cleland, and J. M. Martinis, Appl. Phys. Lett. **95**, 233508 (2009).
[20] C. M. Folkman, J. Podkaminer, K-H. Cho, and C. B. Eom, "Growth of metal/oxide epitaxial heterostructures using PLD and magnetron sputtering with in situ RHEED" (unpublished).
[21] A. J. H. Rijnders, G. Koster, D. H. A. Blank, and H. Rogalla, Appl. Phys. Lett. **70**, 1888 (1997).
[22] P. E. Frieberthauser and H. A. Notarys, J. Vac. Sci. Technol. **7**, 485 (1970).
[23] X. Lai, C. C. Chusuei, K. Luo, Q. Guo, and D. W. Goodman, Chem. Phys. Lett. **330**, 226 (2000).
[24] M. v. Schickfus and S. Hunklinger, Phys. Lett. A **64**, 144 (1977).